韓國水資源學會論文集
第30卷 第6號 · 1997年 12月
pp. 661~669

越流에 의한 非粘着性 堤體에서의 流體-固體 混合流의 水理特性

Hydraulic Characteristics of Fluid-Granule Mixed Flow in Embankment of Noncohesive Materials Due to Overflow

김 진 홍*
Kim, Jin Hong

Abstract

This paper presents a theoretical analysis for a velocity profile of fluid-granule mixed flow and a sheet erosion of an embankment having noncohesive materials due to overflow. The velocity profile were obtained using the stress-strain relationships based on a grain-inertia regime and an erosion depth was obtained using dynamic Coulomb criterion. Experiments were performed to compare with theoretical values and fairly good agreements were found. Theoretical results on velocity profiles, which can be applied to any type of velocity profiles in a fluid-granule mixed flow, showed a considerable improvement for the existing theories on a debris flow. For a design purpose, formulas and figure diagrams for obtaining a velocity profile, an erosion depth, an overflow depth and a granular discharge were proposed for given values of a flood discharge, particle properties and embankment scale.

Keywords: fluid-granule mixed flow, sheet erosion, grain-inertia regime, debris flow

요 지

본 연구에서는 홍수시 비점착성 제체 위를 월류하는 흐름에 의한 유체-고체 혼합류의 속도 분포와 판박형 세굴을 다루고 있다. 속도 분포는 입자-관성 법칙을 기초로 한 응력-변형률 관계식으로부터 구할 수 있었으며, 세굴 깊이는 Coulomb의 동역학적 법칙을 이용하여 구할 수 있었다. 상기 이론으로부터 구한 이론치를 검토하기 위해 실험을 실시하였으며, 실험치와 비교적 잘 일치함을 알 수 있었다. 본 연구에서 얻어진 속도 분포의 이론식은 유체-고체 혼합류의 여러 유속 분포에 모두 적용 가능한 것으로서, 토석류에 관한 기존 이론을 상당히 개선시킬 수 있는 식으로 평가되었다. 설계 목적을 위해서, 만약 홍수량과 입자의 성질 및 제체의 규격이 주어지면, 속도 분포와 세굴 깊이, 월류 수심 및 토사 유출량을 구할 수 있는 식 및 도표를 제시하였다.

핵심용어: 유체-고체 혼합류, 판박형 세굴, 입자-관성 법칙, 토석류

* 광주대학교 공과대학 토목공학과 조교수

1. Introduction

At a river mouth or at the front side of a sluice gate in a diversion dam, sands accumulate and block or reduce the conveyance of the channel (Miwa, 1990). In order to secure the sufficient conveyance of the channel, the artificial flushing is sometimes tried by opening a sluice. Furthermore, flood is a good opportunity for the flushing of accumulated sands (Kim et al., 1989).

Although physical features on the flushing process and their experimental results have been investigated by some authors (Hanes and Inman, 1985; Kato et al., 1985; Shao et al., 1990), the theoretical approaches have not been established yet. Flushing process of a sand embankment due to overflow can be analyzed by the concept of the dilatant model which was initially proposed by Bagnold (1954). The dilatant model is based on the grain-inertia regime where the momentum transfer is made through collisions of sand particles and the shear stress is essentially due to a grain interaction (Bagnold, 1954). He proved the existence of the dispersive pressure resulting from the exchange of momentum between the grains in neighboring layers and proposed the formulas on the dilatant model relating the dispersive pressure with the shear stress. Extensive studies on the dilatant model were carried out by several authors. A comprehensive survey of the mechanics for the dilatant model was given by Savage (1984). Physical phenomena of flushing process and a sediment motion by overtopping flows over an sand embankment were studied by Kim (1997) using the concept of the dilatant model. Since the overflow corresponds to a rapid debris flow with sufficient water to disperse sand grains uniformly throughout the whole depth, theoretical analysis and the mathematical expressions were established using this concept (Kim, 1997).

The main purpose of this study is to formulate the mathematical expressions for the velocity profile of a fluid-granule mixed flow and for the sheet erosion of a sand embankment due to overflow.

2. Experimental Apparatus and Results

A series of experiments in a movable model was performed to investigate the flushing process of a sand embankment (Kim, 1997). Fig. 1 shows an experimental arrangement. An embankment was made of sands inside the recirculating channel of 0.4m wide and 10m long. The median diameter of sands is about 0.5mm. The side wall of the channel was made of glass and a transparent scale was attached to the side wall to see the flushing process well. The channel discharge which is controlled by a valve in a feed back loop could be measured with a manometer attached to a return pipe. Since the flushing time of an embankment was very short, about 50 seconds, a video camera and a time-lapsed video tape recorder were used to measure the flushing rates. A strong light was also used to see the flushing process clearly. Measurements through a video recording were carried out every 10 seconds in order to estimate the flushing rates and thus to investigate the relationship between the inflow discharge and these rates.

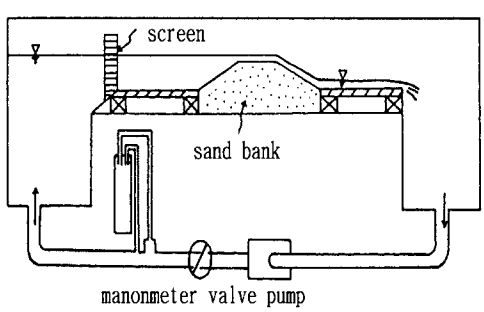

Fig. 1. Experimental Arrangement

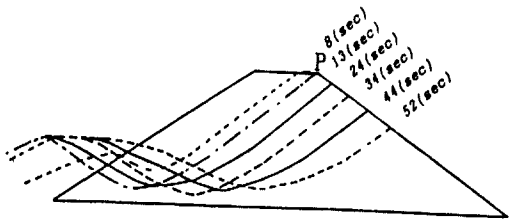

Fig. 2. Time Development of the Flushing Process

Fig. 2 shows the typical case on the time development of the flushing process in a sand embankment with no tail-water condition. Flow over an embankment at an upper part forms a rapid supercritical flow on a steep slope. The tractive stress is very large, resulting in a high erosion potential. Accordingly, a sheet erosion occurs due to the high shear stress, which is characterized by the removal of a layer with certain thickness of a embankment slope. At the downstream part, a deposition occurs due to a release of a embankment slope and a hump is formed as a result. The hump becomes larger with time while the upstream sheet erosion proceeds. But its height remains almost constant after the erosion reaches to an upstream crown point P of an embankment, which corresponds to a flushing profile at 13 seconds from the beginning shown in Fig. 2. This means that the deposition occurs only at the front side of the hump. The eroded sand particles at an upper part of a sand embankment do not spread out to a whole flowing layer since the erosion is not fully developed, and hence two layers exist where the upper layer is a pure water and the sub-layer is a sand-water mixture. The volume fraction of a sub-layer is relatively high due to the large tractive force on a steep slope. Momentum transfer is made through the collisions of sand particles at this sub-layer, and hence the grain-inertia regime on a fluid-granule mixed flow can be assumed

Table 1. Results of the Experimental Data

run no.	q_f(gr/cm·s)	q_s(gr/cm·s)	h_0 (cm)	h (cm)	u_* (cm/s)	T_* (-)	q_{s*} (-)
R1	106	85.18	0.5	0.84	16.13	3.22	39.85
R2	180	144.65	0.5	0.84	16.13	3.22	67.68
R3	300	241.09	0.7	1.18	19.12	4.52	95.16
R4	400	321.45	0.8	1.34	20.37	5.13	119.10
R5	550	442.00	0.8	1.34	20.37	5.13	163.76
R6	600	482.18	0.8	1.34	20.37	5.13	178.65
R7	600	482.18	1.0	1.68	22.81	6.44	159.94
R8	1000	803.64	1.0	1.68	22.81	6.44	265.90
R9	1000	803.64	1.2	2.02	25.01	7.44	242.51
R10	2200	1768.00	1.5	2.52	27.94	9.66	477.57
R11	2500	2009.09	1.5	2.52	27.94	9.66	542.70
R12	3600	2893.09	1.8	3.02	30.58	11.57	714.02
R13	4100	3294.91	1.8	3.02	30.58	11.57	813.19
R14	4200	3375.27	2.0	3.36	32.26	12.87	789.64
R15	5000	4018.18	2.0	3.36	32.26	12.87	940.05
R16	5700	4178.91	2.0	3.36	32.26	12.87	977.65
R17	6000	4821.82	2.2	3.70	33.85	14.17	1075.07
R18	6500	5223.64	2.2	3.70	33.85	14.17	1164.66

considering the Bagnold (1954)'s theory. A depth of an overflow water is nearly constant along the erosion slope in this region supporting the approximation of a uniform flow.

Table 1 shows the data for the experimental results, where q_f is a fluid discharge, q_s is a granular discharge, h_0 is an overflow depth, h is a depth of a shear layer, u_* is a friction velocity, T_* is a non-dimensional shear stress and q_{s*} is a non-dimensional granular discharge.

3. Governing Equations of Fluid-Granule Mixed Flow

3.1 Volume Fraction Profile and Erosion Depth

Consider a two-dimensional steady flow with a constant overflow depth down along an upper part of a sand embankment inclined at an angle θ, to the horizontal with no tail-water condition where an erosion occurs parallel to an initial embank-ment slope as shown in

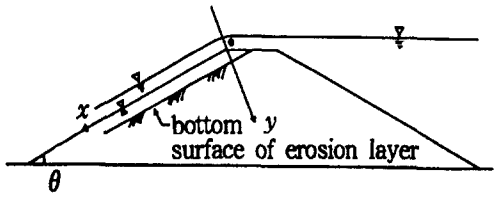

Fig. 3. Two-Dimensional Steady Flow down along an Upper Part of Sand Embankment

Fig. 3. Here the embankment slope θ must be less than the dynamic friction angle ϕ_D for the erosion to occur parallel and for an overflow depth to be constant along a embankment slope. Otherwise the overflow is accelerated and the erosion rate is increased. Experimental observations of the depth profiles on the overflow water flowing down a embankment slope showed that the overflow depth at an upper part of the slope was almost constant illustrated in section 2. Therefore an uniform flow and no net flux of sands in the y-direction can be assumed (Kim, 1997). Considering the above concepts, following two momentum equations and the distribution of the volume fraction on the fluid-granule mixed flow at the upper part of the embankment were obtained as (Kim, 1997),

$$-T_{xy}=(\Delta\rho\, l_1 y+\rho_f y-\rho_f h_0)\, g\sin\theta \tag{1}$$

$$-T_{yy}=\Delta\rho\; g\; l_1\; y\cos\theta \tag{2}$$

$$(N-N_0)^{1/2}=\frac{k_2}{3}y^{3/2},\quad (N_b-N_0)^{1/2}=\frac{k_2}{3}h^{3/2},$$

$$\frac{N-N_0}{N_b-N_0}=\left(\frac{y}{h}\right)^3 \tag{3}$$

where T_{xy} is a granular shear stress, T_{yy} is a granular normal stress, $\Delta\rho$ is a granular submerged density, ρ_s is a granular density, ρ_f is a fluid density, k_2 and l_1 are constants, N is a granular volume fraction, N_0 is a granular volume fraction at a top of mixture layer at $y=0$, N_b is a granular volume fraction at a bottom of a mixture layer at $y=h$.

In order to obtain the depth of a shear layer, i. e., the erosion depth, the dynamic Coulomb criterion can be used as (Takahashi, 1982),

$$T_{xy(y=h)}=T_{yy(y=h)}\cdot\tan\phi_D \tag{4}$$

Eqn. (4) means that the driving force, T_{xy} becomes equal to the resisting force, $T_{yy}\tan\phi_D$ at the level of an erosion depth, h.

Fig. 4 shows the vertical profiles of the driving force and the resisting force over the depth. Definition for the erosion depth can also be explained in Fig. 4. In Fig. 4(a), it can be seen that the erosion occurs to the depth, h until the driving force becomes equal to the resisting force. In this case, the erosion depth is finite. But in Fig. 4(b), the erosion depth becomes infinite since the driving force is larger than the resisting force and the slopes of these two forces are parallel.

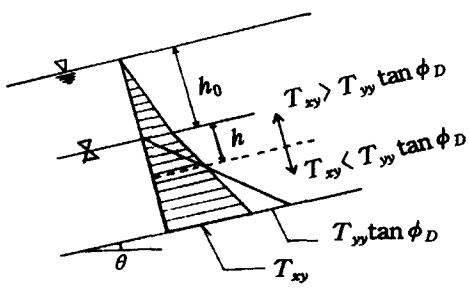

(a) Finite Case

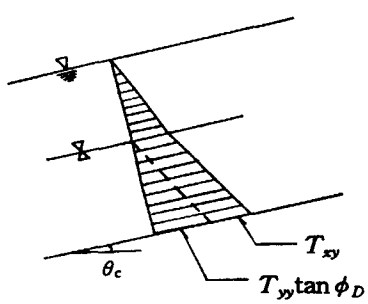

(b) Infinete Case

Fig. 4. Definition Sketch for the Erosion Depth

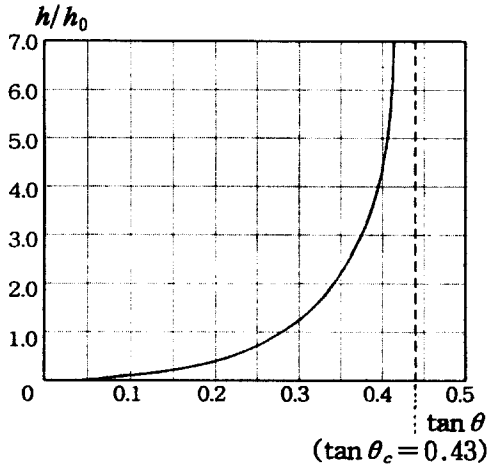

Fig. 5. Non-Dimensional Form of the Erosion Depth

Using Eqns. (1) and (2), Eqn. (4) becomes,

$$\frac{h}{h_0} = \frac{\rho_f \tan\theta}{(\Delta\rho\, l_1+\rho_f)\tan\theta-\Delta\rho l_1 \tan\phi_D} \tag{5}$$

Eqn. (5) is the non-dimensional expression of an erosion depth and it is shown in Fig. 5 as a function of an embankment slope. Here, $\tan\phi_D$=0.89 and l_1=0.575 were used as representative values. In Fig. 5, h/h_0 becomes infinite when the embankment slope approaches to the critical slope θ_c. Here the critical slope is defined as that when the denominator in Eqn. (5) becomes zero corresponding to the slopes of the driving force and the resisting force become parallel shown in Fig. 4(b),

$$\tan\theta_c = \frac{\Delta\rho\, l_1}{\Delta\rho\, l_1 + \rho_f}\tan\phi_D \tag{6}$$

Using Eqns. (3) and (5), the volume fraction at the bottom surface, N_b becomes as,

$$N_b=(\frac{k_2}{3}h^{3/2})^2+N_0 \tag{7}$$

$$=\frac{{k_2}^2}{9}[\frac{\rho_f\tan\theta h_0}{(\Delta\rho\, l_1+\rho_f)\tan\theta-\Delta\rho l_1\tan\phi_D}]^3+N_0$$

The average volume fraction, $\overline{N}$ is,

$$\overline{N}=\frac{1}{h}\int_0^h N dy$$

$$=\frac{1}{h}\int_0^h(\frac{{k_2}^2}{9}y^3+N_0)dy=\frac{{k_2}^2}{36}h^3+N_0 \tag{8a}$$

Hence,

$$\frac{\overline{N}-N_0}{N_b-N_0}=\frac{1}{4},\quad \overline{N}=\frac{3N_0+N_b}{4} \tag{8b}$$

3.2 Velocity Profile

The stress-strain relationship based on the grain-inertia regime is given as (Shibata and Mei, 1986),

$$T_{xy}=-\beta_1(\frac{N_\infty-N_0}{N_\infty-N})^8(\frac{\partial u}{\partial y})^2+\rho_f g h_0\sin\theta \tag{9}$$

where β_1 is a granular viscosity and N_∞ is the volume fraction at the densest packing.

Using Eqns. (1) and (9), the following equation can be obtained,

$$\beta_1(\frac{N_\infty-N_0}{N_\infty-N})^8(\frac{\partial u}{\partial y})^2=(l_1\Delta\rho+\rho_f)gy\sin\theta \tag{10a}$$

$$\frac{\partial u}{\partial y}=-[\frac{(l_1\Delta\rho+\rho_f)g\sin\theta}{\beta_1}]^{1/2}$$

$$(\frac{N_\infty-N}{N_\infty-N_0})^4 y^{1/2},\quad (\frac{\partial u}{\partial y}<0) \tag{10b}$$

Introducing a variable $\hat{y}=(y/h)^{3/2}$, Eqn. (10b) becomes,

$$du=-\frac{2}{3}{k_4}^{1/2}h^{3/2}\sum_{j=0}^{4}{}_4C_j(-k_3\,\hat{y}^2)^j d\hat{y} \tag{10c}$$

where $k_3=(N_b-N_0)/(N_\infty-N_0)$

and $k_4=[(l_1\Delta\rho+\rho_f)g\sin\theta]/\beta_1$ (10d)

Integration of the Eqn. (10c) with no-slip condition u=0 at $\hat{y}$=1 gives,

$$u=\frac{2}{3}{k_4}^{1/2}h^{3/2}\sum_{j=0}^{4}B_j\,[1-\hat{y}^{(2j+1)}] \tag{11a}$$

where, $B_j=\frac{{}_4C_j(-k_3)^j}{2j+1}$ (11b)

The surface velocity, u_0 at $\hat{y}$=0 is,

$$u_0=\frac{2}{3}{k_4}^{1/2}h^{3/2}\sum_{j=0}^{4}B_j \tag{12}$$

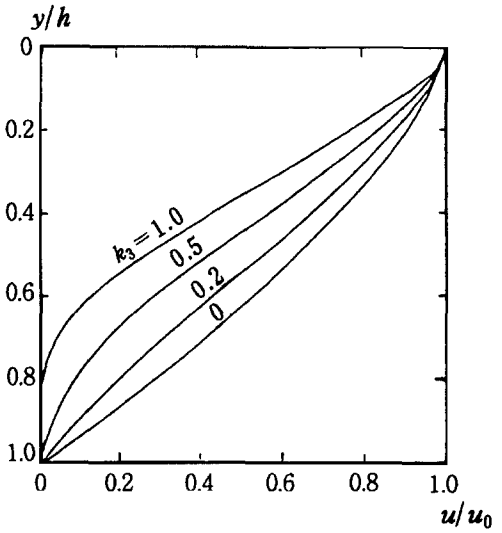

Fig. 6. Non-Dimensional Velocity Profile (Theoretical Value)

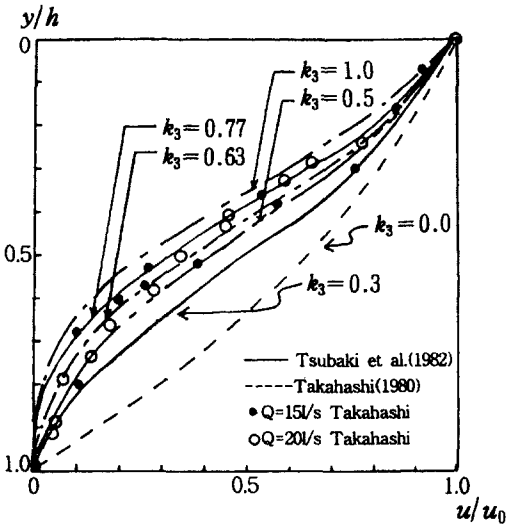

Fig. 7. Non-Dimensional Velocity Profile (Theoretical and Experimental Value)

So, the non-dimensional velocity profile becomes

$$\frac{u}{u_0} = \sum_{j=0}^{4} B_j \left[1 - \hat{y}^{(2j+1)}\right] \Big/ \sum_{j=0}^{4} B_j \qquad (13)$$

Fig. 6 shows Eqn. (13) for some different values of k_3. Here the velocity profile is divided into two types such as,

1) type 1 which is characterized by upward convex near the bottom of a shear layer and downward convex near the top surface of a shear layer in case k_3=1.0 and 0.5. This type is similar to that of Tsubaki et al. (1982).

2) type 2 which is characterized by downward convex over the whole shear layer in case k_3=0.2and 0.0. This type is similar to that of Takahashi (1980)'s theore-tical curve.

If k_3=0.2, the non-dimensional velocity profile becomes,

$$\frac{u}{u_0} = 1 - \hat{y} = 1 - \left(\frac{y}{h}\right)^{3/2} \qquad (14)$$

Eqn. (14) is the same as that of Takahashi (1980)'s theoretical curve.

Fig. 7 shows the non-dimensional velocity profile obtained from the results of Takahashi(1980) and Tsubaki et al.(1982). Here the solid line is the theoretical result by Tsubaki et al. (1982) and the dotted line is the Takahashi (1980)'s theoretical one. Comparing Fig. 6 and Fig. 7, the solid line corresponds to the curve of k_3=0.3, the dotted line corresponds to that of k_3=0.0 and the experimental values exist between the lines of k_3=0.5 and 0.1 Takahashi (1980) could not explain the discrepancy between the theoretical results and the experimental ones with respect to k_3. The non-dimensional velocity profile obtained in this study can explain this discrepancy and hence can be applied to any type of velocity profiles in a fluid-granule mixed flow, which showed a considerable improvement for the existing theories on a debris flow.

The average velocity $\bar{u}$ is given as,

$$\bar{u} = \frac{1}{h} \int_0^h u(y)dy \qquad (15a)$$

If we introduce a variable $y_0 = y/h$, then the above equation becomes,

$$\bar{u}=\frac{2}{3}k_4^{1/2}h^{3/2}\sum_{j=0}^{4}B_j\left(1-\frac{1}{3j+2.5}\right) \quad (15b)$$

3.3 Granular and fluid discharge

Granular discharge, q_s can be obtained using Eqns. (3) and (11a) and using a variable $y_0=y/h$ as follows,

$$q_s=\rho_s\int_0^h N(y)\,u(y)\,dy$$

$$=\rho_s\int_0^1 \{(N_b-N_0)\,y_0^3+N_0\}\,[\frac{2}{3}k_4^{1/2}h^{3/2}\sum_{j=0}^{4}$$

$$\bar{u}=\frac{2}{3}k_4^{1/2}h^{3/2}\sum_{j=0}^{4}\frac{4Cj(-k_3)^j}{2j+1}\left(1-\frac{1}{3j+2.5}\right)$$

$$B_j\,\{1-y_0^{(3j+1.5)}\}\,]h\,dy_0=\frac{2}{3}\rho_s k_4^{1/2}h^{5/2}\sum_{j=0}^{4}$$

$$[B_j(\bar{N}-\frac{N_b-N_0}{3j+5.5}-\frac{N_0}{3j+2.5})] \quad (16)$$

Non-dimensional form of Eqn. (16) is,

$$q_{s*}=q_s/\rho_s u_* d=\frac{2}{3}k_4^{1/2}h^2\sum_{j=0}^{4}$$

$$[B_j(\bar{N}-\frac{N_b-N_0}{3j+5.5}-\frac{N_0}{3j+2.5})]\Big/\sqrt{g\sin\theta}\,d \quad (17)$$

where $u_*(=\sqrt{gh\sin\theta})$ is a friction velocity and d is a particle diameter.

Fig. 8 shows Eqn. (17) as a function of non-dimensional shear stress, T_* in case $\beta_1\times 10^4=8.6$, where β_1 is the granular viscosity included in k_4 as shown in Eqn. (10d). Then T_* is defined as,

$$T_*=\frac{u_*^2}{(\frac{\rho_s-\rho_f}{\rho_f})gd} \quad (18)$$

In Fig. 8, the solid line represents the theoretical value of Eqn. (17) and the dotted lines represent Takahashi(1982)'s theoretical values for some different values of θ. The solid line is consistent with the dotted line of $\theta=6^\circ$. Fairly good agreements can be seen although the erosion rate of present study is larger than that of Takahashi(1982)'s and

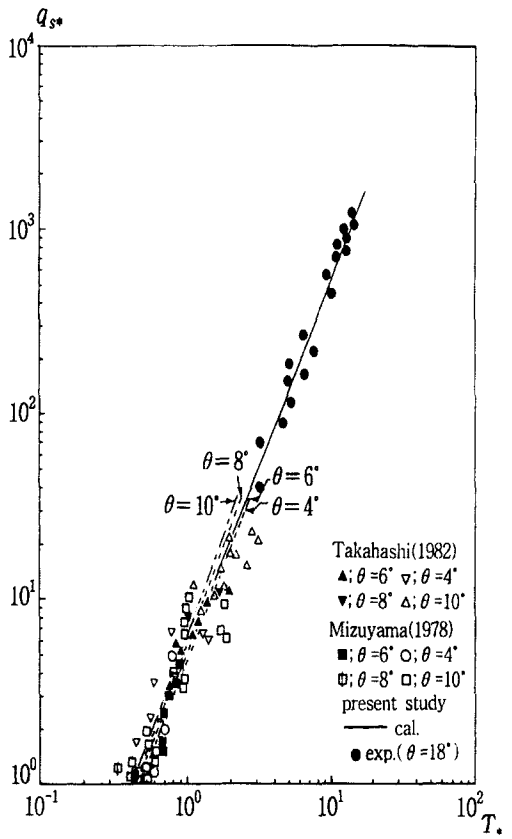

Fig. 8. Non-Dimensional Granular Discharge

Mizuyama(1978)'s experimental data. The effect of a slope angle is small as a whole in the range of the debris flow where T_* is larger than0.4 (Takahashi, 1982).

Fluid discharge, q_f is calculated as follows,

$$q_f=-\rho_f h_0 u_0+\rho_f\int_0^h \{1-N(y)\}\,u(y)\,dy$$

$$=\frac{2}{3}k_4^{1/2}h^{5/2}\{(\Delta\rho l_1\cdot\frac{\tan\phi_D-\tan\theta}{\tan\theta}+\rho_f)\sum_{j=0}^{4}B_j$$

$$+\rho_f\sum_{j=0}^{4}B_j(1-\bar{N}+\frac{N_0-1}{3j+2.5}+\frac{N_b-N_0}{3j+5.5})\} \quad (19)$$

Fig. 9 shows Eqn. (19) with varying value of β_1. It can be seen that the experimental values exist around the curve of $\beta_1\times 10^4=8.6$ and we can estimate the erosion depth for

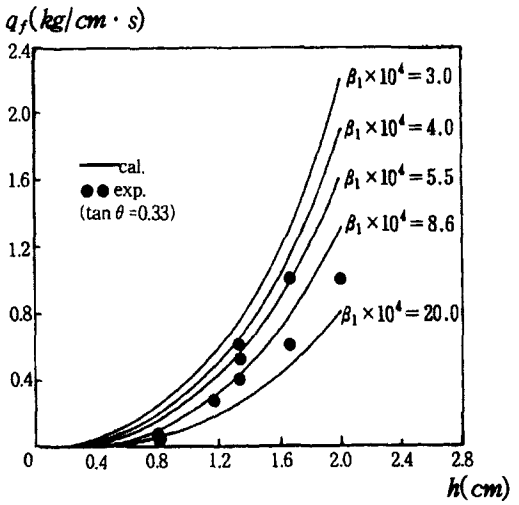

Fig. 9. Fluid Discharge as a Function of the Erosion Depth

given value of the fluid discharge, i. e., the flood inflow.

For a computational procedure, if the flood inflow discharge, an embankment size and particle properties are given, we can estimate:

(1) the erosion depth by Eqn. (19) or Fig. 9,

(2) the overflow depth by Eqn. (5) or Fig. 5,

(3) the velocity profile by Eqn. (13) or Figs. 6 and 7,

(4) the granular discharge by Eqns. (16) and (17) or Fig. 8.

4. Conclusions

Theoretical analysis for a velocity profile of fluidgranule mixed flow and a sheet erosion of an embankment having noncohesive materials due to overflow were studied and compared with the experimental values. From these results, the following conclusions were obtained.

(1) The velocity profile was obtained using the stress-strain relationships based on a grain-inertia regime. It was applied to any type of velocity profiles in a fluid-granule mixed flow, which showed a considerable improvement for the existing theories on a debris flow.

(2) The erosion depth was obtained using the dynamic Coulomb criterion, where the erosion occurs to the depth level until the driving force becomes equal to the resisting force.

(3) The volume fraction at the bottom surface of the fluid-granule mixed flow and the average volume fraction were obtained with the given value of the erosion depth.

(4) The granular discharge and the erosion depth obtained from the theoretical analysis were compared with the experimental values and fairly good agreements could were found. From this, the erosion depth and the granular discharge were estimated if the value of flood discharge is known.

(5) For a design purpose, formulas and figure diagrams for obtaining a velocity profile, an erosion depth, an overflow depth and a granular discharge were proposed for given values of a flood discharge, particle properties and embankment scale.

References

Bagnold, R.A. (1954). "Experiments on a gravity free dispersion of large solid spheres in a Newtonian fluid under shear." *Pro. of Roy. Soc.* London, A225, pp. 49-63.

Hanes, D.M. and Inman, D.L. (1985). "Observations of rapidly flowing granular-fluid materials." *J. Fluid Mech.* Vol. 150, pp. 357-387.

Kato, Y., Hashimoto, H. and Fujita, K. (1985). "Experimental study on levee reinforcement against failure by overtopping." *Pro. of 29th Hydraulic Conference*, JSCE, pp. 627-632

Kim, J.H. (1997). "Flushing process by overtopping flows over sand embankment." *Pro. of 7th International Conference on Computing in Civil and Building Engineering*, Seoul, pp. 85-92.

Kim, J.H., Tamai, N., and Asaeda, T. (1989). "Bank erosion due to overflow" *Pro. of 45th Annual Conference*, JSCE, pp. 423-424.

Miwa, H. (1990). "Process of flushing sand accumulated under gates on a dam by sluice outlet." *Pro. of 34th Hydraulic Conference*, JSCE, pp. 247-252.

Mizuyama, T. (1978). "Sedimentation and sediment flow on inclined surfaces." *J. Fluid Mech.*, Vol. 212, pp. 139-153.

Savage, S.B. (1984). "The mechanics of rapid granular flows." *Advances in Applied Mechanics*, 24, Edited by Wu, T.Y. and Hutchinson, J., Academic Press, pp. 289-366.

Shao, X., Tanaka, H. and Shuto, N. (1990). "Experimental study on scouring of a sand bar by overflow." *Pro. of 34th Hydraulic Conference*, JSCE, pp. 373-378.

Shibata, M., and Mei, C.C. (1986). "Slow parallel flows of a water-granule mixture under gravity, part 1: Continuum modeling." *Acta Mechanica*, 63, Edited by Bailard, J.A. and Mortimer, C.H., Springer-Verlag, Massachussetts, pp.179-193.

Takahashi, T. (1980). "Debris flow on prismatic open channel." *J. Hydr. Div.*, ASCE, Vol. 196, pp. 381-396.

Takahashi, T. (1982). "Debris flow." *Annual Review of Fluid Mechanics*, 13, Edited by Batchelor, G.K. and Miles, J.W., Cambridge University Press, Cambridge, pp. 57-77.

Tsubaki, T., Hashimoto, H. and Suetsugi, T.(1982). "Grain stress and flow properties of debris flow." *Pro. of 38th Annual Conference*, JSCE, pp. 79-91.

〈최종본 접수일 : 1997년 10월 22일〉